Proceedings of the 7th International Young Geotechnical Engineers Conference – Scott (Ed.)

Strain localization in a triaxial extension test on transparent sand

Localisation des déformations dans un essai d'extension triaxiale sur sable transparent

David H Marx & Jorge G Zornberg
Department of Civil, Architectural and Environmental engineering, The University of Texas at Austin, United States of America, dawie.marx@utexas.edu

ABSTRACT: Triaxial extensions tests were done on a poorly graded transparent sand at 100 kPa confining stress to study the occurrence of strain localization. The transparent sand was manufactured by saturating fused quartz with a mineral oil mixture. A laser was used to illuminate a plane through the sample. Particle movement along this plane was tracked using digital image correlation. Strain localization first occurred in the region of the specimen that eventually necked. However, the shear bands were not confined to that region and also drifted to the bottom of the specimen. Slip-stick behaviour, which is typical to transparent sand, was also observed. It was found that the strain localized only during "slip"-events. Between the slip events the sample stabilized, and no strain localization was apparent.

RÉSUMÉ : Des essais d'extensions triaxiales ont été effectués sur un sable transparent mal classé à une contrainte de confinement de 100 kPa. Le sable transparent a été fabriqué en saturant du verre de quartz avec de l'huile minérales. Un laser a été utilisé pour éclairer un plan à travers l'échantillon. Le mouvement des particules le long du plan analysé a été suivi en utilisant la corrélation numérique d'images. La concentration des déformations s'est premièrement produite dans la région de l'échantillon qui a été rétrécie. Pourtant, les bandes de cisaillement n'étaient pas confinées à cette région et dérivaient également vers la partie inférieure de l'échantillon. Un comportement collé-glissé typique du sable transparent a également été observé. Il a été constaté que la déformation locale n'avait pas lieu que lors d'événements de « glissement ». Entre les événements de glissement, l'échantillon s'est stabilisé et aucune concentration de contraintes a été observée.

KEYWORDS: fused quartz, digital image correlation, transparent sand, triaxial extension

1 INTRODUCTION

Routine triaxial tests are typically done in compression. That is, the axial stress is the major principal stress while the radial stress is the minor principal stress. Alternatively, in a triaxial extension test the axial stress is the minor principal test and the radial stress is the major principal stress. The most common version of the extension test is an unload test, i.e. the axial stress is reduced while the confining stress is kept constant. For both triaxial compression and extension tests the intermediate principal stress is equal to the radial stress.

The triaxial extension test simulates stress states not represented by triaxial compression, e.g. heave at the bottom of an excavation (Bishop & Henkel 1962), passive earth pressure, tunnel roofs, (Wu & Kolymbas 1991) or the toe of a slope (Sadrekarimi 2014).

The strain in the specimen during a conventional triaxial extension test is highly variable (Yamamuro & Lade 1995). Consequently, the results of triaxial extension and compression tests cannot readily be compared (Roscoe et al 1964). Furthermore, strain localization tends to occur for a wide range of confining stresses for both soils with contractive and dilative tendencies (Yamamuro & Lade 1995). This unstable behaviour contributes to large scatter in the results.

In conventional triaxial extension tests the occurrence of strain localization is typically inferred from the shape of the deformed specimen after failure. However, in this paper strain localization is studied by measuring the internal particle movement, during shear, using transparent sand.

2 METHODOLOGY

Triaxial extension tests were done on oil-saturated samples of sand-sized fused quartz. Images were captured of a laser-illuminated plane through the sample. Subsequently, these images were analysed using Digital Image Correlation (DIC) to measure the development of strain localization across the plane.

2.1 *Test setup and procedure*

The triaxial extension tests were done on two, identical 50 mm diameter, 100 mm tall specimens of fused quartz. Enlarged platens (75 mm diameter) with lubricated ends consisting of two layers of greased, black silicone discs were used. A small tube in the centre of each platen was used for drainage and to anchor the specimens (Vernese & Lee 1977). Transparent membranes were constructed from clear silicone sheets.

An automated triaxial system consisting of a load frame and two volume pumps was used. The pumps were connected to two bladder accumulators that were used to apply back pressure and confining stress to the specimens. Oil was used both to saturate the specimens and as a confining liquid.

The deviatoric stress was measured with a 444 N (100 lb), external loadcell. This loadcell was connected to the top of the loading ram using a tension coupling. A threaded connection was used between the bottom of the loading ram and the top cap.

After back pressure saturation to 300 kPa a B-value check was performed, and the samples were visually inspected for air bubbles. Subsequently the samples were consolidated to 100 kPa effective stress. Finally, the samples were sheared under drained conditions by reducing the vertical stress at an axial strain rate of 6%/hour. This, relatively slow rate of shear was dictated by the time required for images to be captured at increments of 0.02% axial strain (see Section 2.2). A diagram of the setup is shown in Figure 1.

2.2 *Fused quartz*

Poorly graded (SP) fused quartz was used to manufacture a transparent sand (Ezzein & Bathurst 2011). The sand has a D_{50} of 2.36 mm, the coefficient of uniformity is 2.8 and the coefficient of curvature is 1.4. Minimum and maximum void ratios of 0.52 and 0.72, respectively, were measured. Each sample was compacted in eight layers and the void ratio at the end of consolidation was 0.56.

The fused quartz was saturated with an oil mixture (in this case a 52% Puretol 7 and 48% Paraflex HT4) with a matching refractive index. Consequently, light transmits through the specimen, rather than refracting. Thus, the specimen is transparent.

A 450-mW laser with a wavelength of 638 nm was used to illuminate a plane through the sample (see Figure 1). Due to a slight refractive index mismatch between the oil and the quartz the edges of the particles are illuminated by the scattered light. Thus, the movement of the particles can be tracked using digital image correlation (see Section 2.3). A Canon EOS 5DS R camera fitted with a Sigma 50 mm f/1.4 lens was used to take photos of the test at 0.02% increments of axial strain.

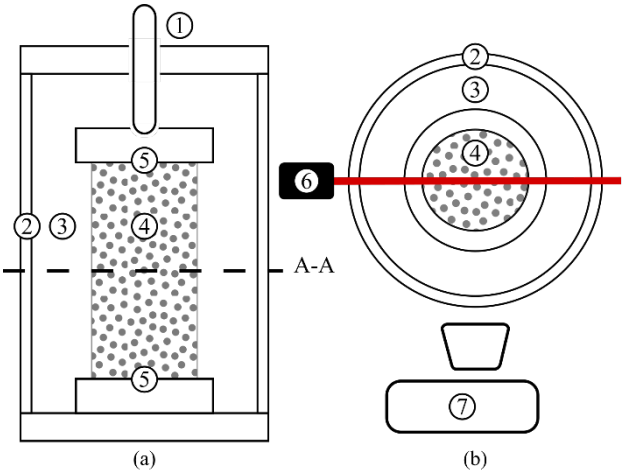

(1) Loading ram (2) Acryllic wall (3) Confining oil (4) Quartz and oil mixture (5) Lubricated platten (6) Laser (7) Camera

Figure 1. Diagram of the experimental setup, a) vertical section, and b) horizontal section.

2.3 *Stress-strain behaviour*

Three different methods were considered for calculating the stress-strain response of the samples. For all three methods discussed the deviatoric stress measured was corrected for the tensile resistance provided by the membrane (Wu & Kolymbas, 1991). A correction for the force due to gravity (Wu & Kolymbas, 1991) was deemed negligible due to the strain localizing at the top of the sample.

For the first method the sample was assumed to deform as a right cylinder. The axial strain ($\varepsilon_{A,C}$) was calculated using the initial sample height and the displacement of the platen. The second method is based on the approach by Roscoe et al. (1964). In this case the global axial strain (ε_A) was calculated using a virtual strain gauge. For the final method a virtual strain gauge was used to calculate the local axial strain ($\varepsilon_{A,L}$) in the region that is actively necking. The latter two methods are discussed in more detail in Sections 3.1.2 and 3.1.3.

2.4 *Digital image correlation and strain fields*

The images of the laser-illuminated plane through the sample were captured in RAW format to retain the maximum amount of detail. These images were subsequently pre-processed and converted to PNG files as discussed in Marx & Zornberg (2022).

Digital Image Correlation (DIC), as implemented in GeoPIV-RG (Stanier et al. 2015), was used to measure the displacement of particles along the illuminated plane, during shear. DIC involves dividing an image in a series of subsets and tracking those subsets through successive images. The movement of the centroids of the subsets can be used to generate a displacement field. This displacement field can subsequently be used to calculate strain fields along the plane under consideration.

The circular subsets used in the analysis were 200 px in diameter, spaced at 50 px intervals. Jones & Iadicola (2018) recommends that each subset should contain at least three DIC features. The D_{50} of the transparent sand tested in this study (2.36 mm) was equivalent to ~75 px.

3 RESULTS

An image of the laser-illuminated section through the first specimen (TXE-1), at the end of the test, is shown in Figure 2a. The specimen clearly necked, and thus severe strain localization can be expected. The second specimen (TXE-2) failed at 4% axial strain due to a puncture in the membrane. However, the strain fields, and visual inspection of the sample, indicated that strain localization was present, and that necking would have occurred at the top of the sample.

The necking occurred at the top of the specimens similar to the results reported by Wu & Kolymbas (1991) for dense specimens. However, that is contrary to the results of Roscoe et al (1964) and Yamamuro & Lade, (1995) that observed necking in the centre of the specimens. Wu & Kolymbas (1991) partly attributed this discrepancy to the use of lubricated ends. Alternatively, the sample weight may result in a lower nett vertical stress at the bottom of the sample. Consequently, the sample will be more likely to fail at the top. An insufficient number of tests were done to confirm this theory.

In the next section the stress-strain behaviour of the two triaxial extension tests are discussed. Thereafter, the strain localization is explored in terms of 1) shear band development with axial strain, 2) strain localization during slip-stick, and 3) progression of the shear band.

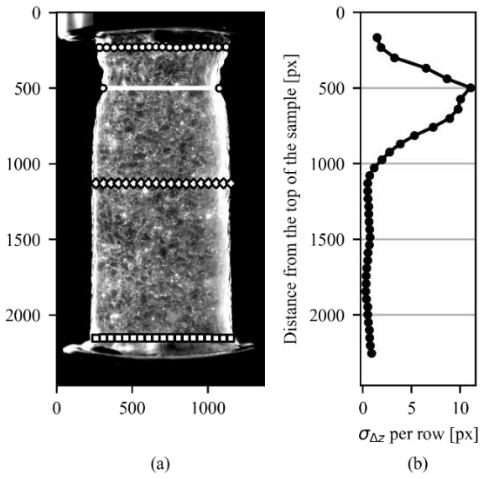

Figure 2. a) Photo of TXE-1 at the end of the test with locations of minimum sample diameter and virtual strain gauges shown: ○ top anchor, □ bottom anchor, ◊ bottom anchor for local measurement. b) Standard deviation of the vertical movement for each row of subsets at the end of the test.

3.1 *Stress-strain behaviour*

The stress-strain curves calculated with the three different methods are discussed in the following sections.

3.1.1 *Method 1: Right cylinder*

Typically, when calculating the deviatoric stress for a triaxial compression specimen it is assumed that the soil deforms as a right cylinder. However, the necking that occurs during triaxial extension tests invalidates this assumption. Nevertheless, as a reference the stress-strain curve for the first triaxial extension test (TXE-1), when assuming that the sample deforms as a right cylinder, is shown in Figure 3. Of interest is that the deviatoric

stress as calculated with this method plateaus after the specimen yields.

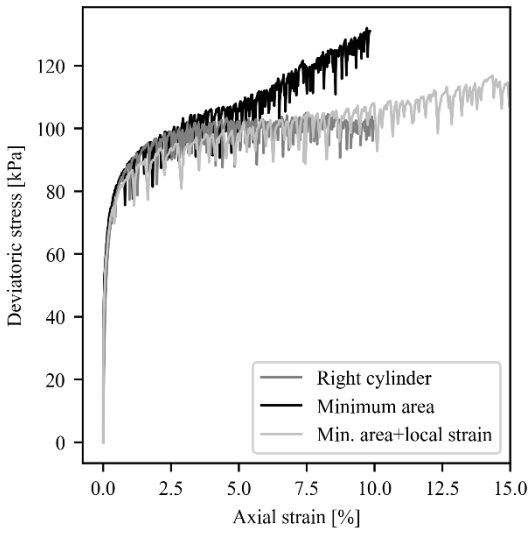

Figure 3. Stress strain curves for TXE-1 calculated with three different methods.

3.1.2 *Method 2: Minimum area*

The second stress-strain curve in Figure 3 ("Minimum area") is based on the approach by Roscoe et al. (1964). The minimum diameter of the sample was measured for each image (see Figure 2 for an example). This corresponding minimum area was used to calculate the deviatoric stress.

For this second analysis the axial strain (ε_A) was calculated from the displacements measured with the DIC analysis. This was done to remove the effect of bedding error. A virtual strain gauge consisting of the average displacement of two rows of subsets was used. The locations of these subsets are indicated on Figure 2 (○ and □).

Initially the axial strain from the DIC-gauge was slightly lower than that calculated from the platen movement. It is assumed that at the start of the test there was some compliance in the system and thus the global measurements included the deformation of both the specimen and the system. At larger platen displacements the axial strain rate calculated from the DIC displacements and that from the platen movement correlated. This corresponds to the results of Wu & Kolymbas (1991) that found the bedding error due to lubricated ends insignificant in triaxial extension tests.

Similar to Roscoe et al (1964), the deviatoric stress calculated considering the minimum sample area continuously increased with axial strain. However, in the results reported by Roscoe et al. (1964) the deviatoric stress increased after yield, plateaued, and then increased again at a higher rate. That plateau is used to define failure. For the results in Figure 3 no distinct plateau is observed. However, the plateau may be obscured by the slip-stick behaviour (rapid decreases and increases in deviatoric stress) of the fused quartz. Slip-stick will be discussed further in Section 3.4.

3.1.3 *Method 3: Min. area + local strain*

The inherent assumption in the axial strain measurements discussed above (DIC and global) is that the axial strain is uniformly distributed through the specimen. This is of course not the case in conventional triaxial extension tests (Roscoe et al, 1964; Wu & Kolymbas, 1987; Yamamuro & Lade, 1995). For the third stress-strain curve the local axial strain ($\varepsilon_{A,L}$) in the region that necked was calculated using a digital strain gauge.

To ensure an accurate measurement by the virtual strain gauge it needs to be anchored at two points on the specimen where the vertical displacement is uniform along the width of the specimen (i.e. no localization is occurring).

Firstly, the standard deviation, of the vertical displacement ($\sigma_{\Delta yz}$) of each row subsets at the end of the test was calculated. As shown in Figure 2, the $\sigma_{\Delta z}$ for the bottom 2/3^{rds} of the specimen was low and constant. Thus, these subsets moved in unison. Closer to the top of the specimen $\sigma_{\Delta z}$ increased, indicating non-uniform, vertical movement, and thus shear strain. The inflection point of the $\sigma_{\Delta z}$-distribution was used as the bottom anchor for this virtual strain gauge. For the top anchor the same row of subsets as for Method 2 was used.

The third curve in Figure 3 ("Min. area + local strain") shows the axial stress calculated for the minimum area as a function of the local axial strain. Similar to the "Minimum area" curve in Method 2 the deviatoric strain continuously increases with axial strain. However, the increase is fairly constant after 2.5% strain without a discernible yield location, i.e., there is no plateau or sudden increase.

Initially, while the specimen was deforming uniformly (and elastically) the local axial strain matched that of the full-sample DIC measurements. However, as the test progressed the local axial strain was significantly higher for a given top cap displacement. This is illustrative of the highly non-linear axial strain throughout the specimen.

3.1.4 *Discussion*

All three methods used to calculate the stress-strain curve has limitations. The "Right cylinder" method ($\varepsilon_{A,C}$) does not represent the physical behaviour of the specimen. However, the procedure gives consistent results that are comparable between different specimens, confining stresses and laboratories.

The "Minimum area" method (ε_A) is potentially a more accurate reflection of the maximum stress inside the sample. However, sophisticated measurements and analysis is required for this method. Furthermore, the axial strain reported is a value averaged across the sample.

The "Min. area + local strain" method ($\varepsilon_{A,L}$) is the best representation of the stress-strain behaviour of the segment of the sample that is actively shearing. However, this method assumes that after strain localization occurred, deformation is limited to the top of the sample. The discussion on shear bands in the subsequent sections will question this assumption. In addition, these measurements are not compatible with the volumetric strain measurements are made for the sample as a whole, and thus are not compatible with these local axial strain measurements.

In Figure 4 the stress strain curves for TXE-1 and TXE-2 are compared to illustrate the repeatability of the tests. The stress-strain curves were both calculated using the "Minimum area" method (ε_A) and illustrates a good match. Subsequent references to axial strain refer to the strain calculated with the "Minimum area" method (ε_A).

Both tests exhibited the slip stick behaviour common to oil-saturated fused quartz (Ezzein & Bathurst 2011). The slip-stick behaviour reflects chains of load-bearing particles forming, collapsing and reforming within the sample. Ezzein & Bathurst (2011) postulates that this same behaviour is also present in water-saturated samples. However, the sheer number of forces chains in a water saturated sample means that the collapse of any single chain does not have a pronounced effect on the measured stress-strain response.

3.2 *Shear band development with axial strain*

In Figure 7 the shear strain that has developed in specimen TXE-1 is shown for different levels of axial strain (marked on Figure 4). The strain fields were calculated from the DIC displacement measurements (see Section 2.3). Each plot shows the shear strain that has accumulated since the previous plot. For example, for Figure 7(a) shows the shear strain that has

developed from $\varepsilon_A = 0.75\%$ to 1.48%. The axial strain measurement was made using Method 2 (ε_A) which resulted in slightly irregular strain increments between different images, and thus plots

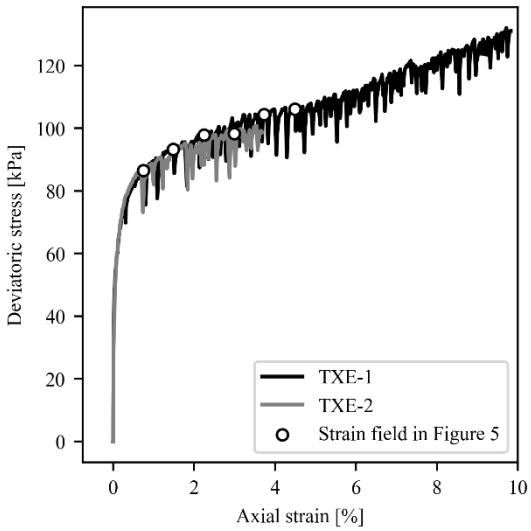

Figure 4. Comparison of stress-strain curves for TXE-1 and test TXE-2 calculated with the minimum area method.

Initially, up to $\varepsilon_A = 0.75\%$, no slip-stick has occurred and the shear strain in the sample is homogeneous. This can be considered a yield point. At $\varepsilon_A = 2.24\%$ irreversible slip-stick has occurred, and strain localization occurs at the region that necked in Figure 2. At $\varepsilon_A = 3.73\%$ a shear band clearly bisects the specimen, and it is possible that the specimen has failed. It would be reasonable to assume that all subsequent shear will occur in this weakened zone.

However, the strain localization does not remain at the top of the specimen; at $\varepsilon_A = 4.49\%$ the strain concentration seems to diffuse from the top of the sample down to the centre. This would imply that the whole sample is actively shearing, rather than only the top half. The axial strain of 4.49% corresponds roughly to the location where the slope of the deviatoric stress increased in Figure 4. To further understand this downwards progression of the shear band the slip-stick behaviour observed in the specimen will first be investigated.

3.3 *Shear strain development during slip-stick*

The slip-stick behaviour first shown in Figures 3 and 4 was further investigated by considering the corresponding shear strain distribution. In Figure 8 the shear strain that accumulated over an ~0.02% axial strain increment (the resolution of the DIC measurements) is shown for two slip-stick events. The corresponding stress-strain extract is shown in Figure 5.

The strain fields in Figure 8 corroborates the theory that "slip-stick" behaviour is due to load bearing particle chains forming and collapsing. While the deviatoric stress increases (e.g. $\varepsilon_A = 2.65\%$ to 2.75%), the load bearing particle chain(s) develops and there limited movement of particles. However, once the capacity of the chain is exceeded ($\varepsilon_A = 2.79\%$) the chain buckles, the deviatoric stress drops (the "slip"-event), significant particle movement occurs, and a shear band is visible. Subsequently, the buckling particles are confined by surrounding particles, the particle movement is halted (the "stick"-event), and there is no more strain localization.

From the intermediate strain fields in Figure 8, it is clear that the majority of the shear strain in the sample occurs during the slip events. Leading to, and following, the slip-event the shear strain in the specimen is slightly biased towards the top, but uniform with no strain localization present.

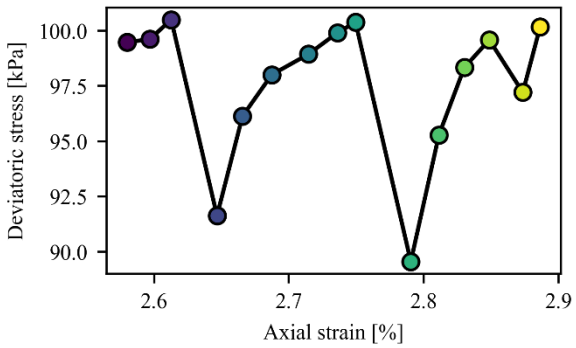

Figure 5. Deviatoric stress versus axial strain (ε_A) for the shear strain fields shown in Figure 8.

3.4 *Progression of strain localization*

The centroid of the shear strain localization in each image was tracked to further investigate the downwards progression of shear bands through the sample. The vertical component of the centroids is shown in Figure 6 as a function of axial strain. The centroids are shown as discrete points as they were only calculated when a distinct shear strain concentration was visible (i.e., for slip events).

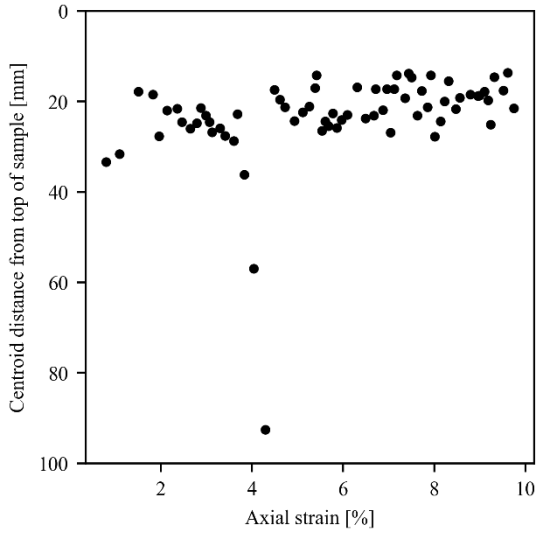

Figure 6. Vertical position of the centroid of the active shear band as a function of axial strain.

In general, there is some noise in the position of the centroid. Nevertheless, up to 3.7% axial strain the shear strain localized at the top of the sample as expected. However, subsequently the centroid abruptly moved towards the bottom of the sample. This also observed in Figure 7(f) where the magnitude of the strain localization at the top of the specimen decreases, while the strain in the bottom halve of the specimen increases. At 4.5% axial strain the concentration is once again at the top of the sample and remained there for the duration of the test.

The shear strain distributions in Figure 9 validates this behaviour. Over an increment of 0.44% axial strain the zone of

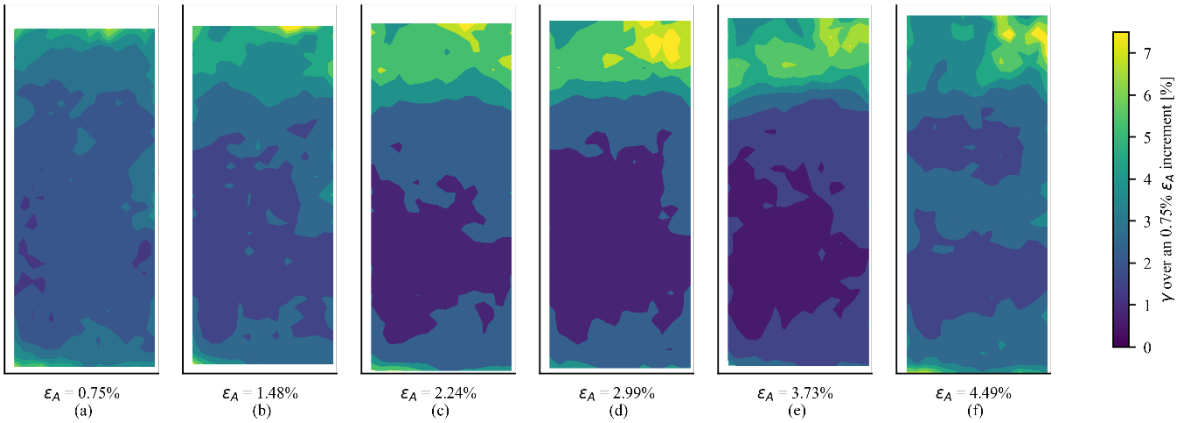

Figure 7. Shear strain that accumulated in the sample over ~0.75% axial strain increments.

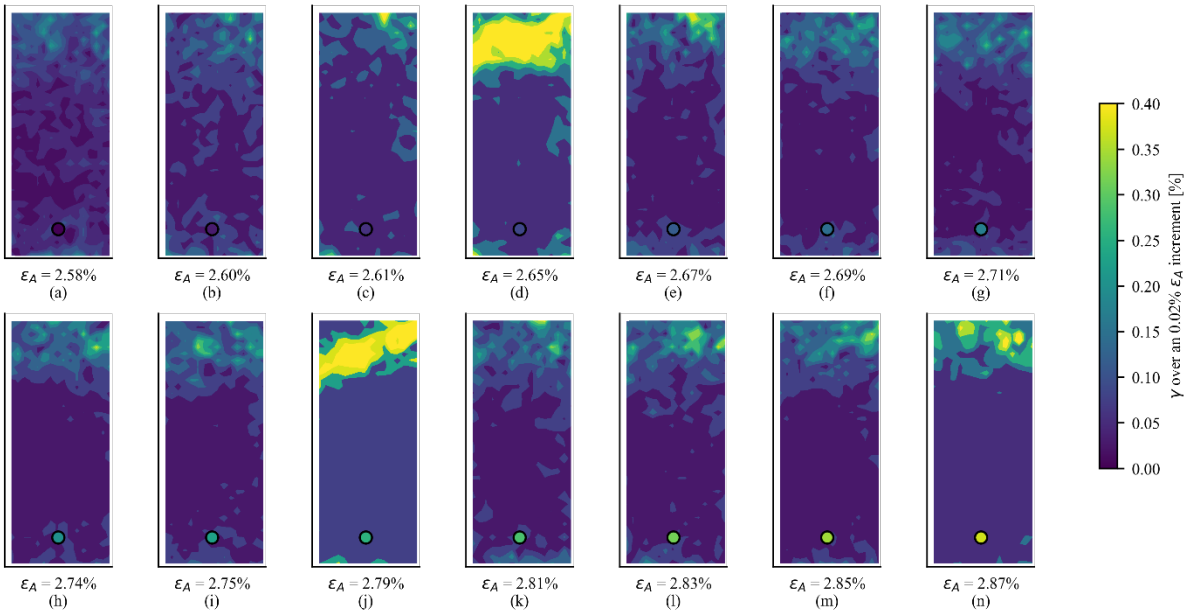

Figure 8. Shear strain accumulated over ~0.02% axial strain increments for two slip-stick events.

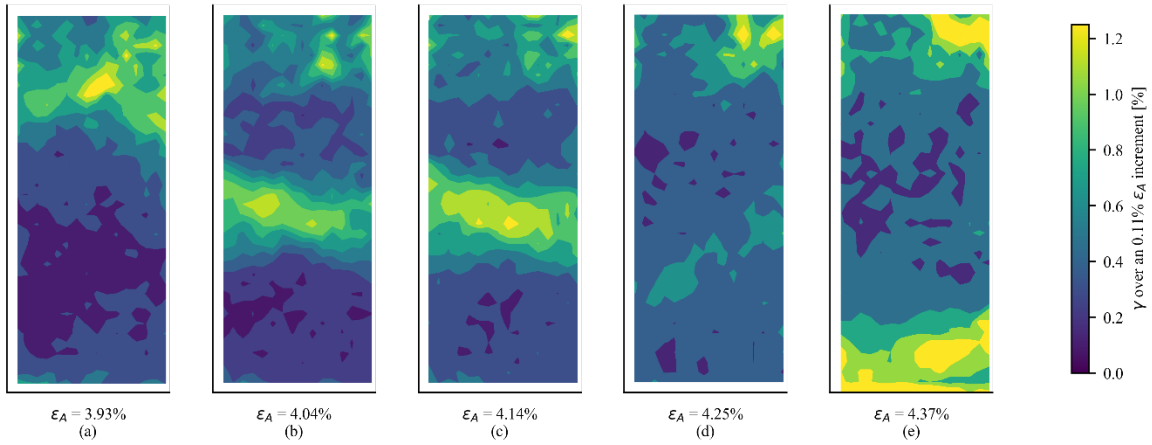

Figure 9. Shear strain accumulated over 0.11% axial strain increments showing the downwards progression of a shear band through a specimen

localized shear strain moves from the top of the sample towards the bottom. It is assumed that at $\varepsilon_a = 4.25\%$ the shear concentration is angled out of plane and thus it is not captured by the DIC. A similar downward migration of the shear strain concentration was apparent in TXE-2. For TXE-1 the downwards progression of the shear band correlated to the inflection in the stress-strain curve in Figure 4. For TXE-2 the membrane punctured shortly after the downward migration of the strain concentration. The downward migration of the shear band might be related to the slip-stick behaviour of the transparent sand. The specimen will always fail along its weakest plane. However, eventually the plane stops slipping as particle movement is constrained by neighbouring particles (the

stick-event). Due to the movement of the particles being constricted the strength of that region is increased.

At some stage in the test the interlock in the necked area of the sample is significant enough that it is stronger than the rest of the sample. Consequently, the load is transferred down through the sample until it reaches a weaker zone. This weak zone slips, stabilizes (sticks) and then transfers the load further down the specimen. Thus, the shear band progressively travels down the specimen. Once the shear band reaches the bottom of the specimen all weak zones have been stabilized. Subsequently, shear once again occurs at the necked region where the deviator stress is the greatest.

Some of the key criticisms against triaxial extension tests is the shear strain localization that results in an unstable test (Yamamuro & Lade, 1995) as well as the non-uniform axial strain distribution (Roscoe 1964). Both these arguments are valid and are clearly supported by the results discussed in this paper. However, it is enlightening to observe that even though strain localized at the top of the sample fairly early in the test it does not result in an abrupt division of the sample. Rather, should a weaker region exist in the bottom of the sample (whether actual, or artificially due to reduced confinement by the membrane), load will be distributed past the middle of the sample, down to the weaker region at the bottom. Thus, the specimen acts as a unit cell even in a triaxial extension test. Accurate interpretation of the governing deviatoric stress, axial strain and effective void ratio is of course an open question.

4 SUMMARY

Triaxial extension tests were done on oil saturated specimens of fused quartz. Both samples exhibited necking near the top of the sample. The stress-strain curve was calculated with three different methods: 1) by assuming the sample deforms as a right cylinder, 2) by considering the minimum area of the sample and 3) by considering both the minimum area and the local axial strain in the specimen.

The stress-strain behaviour of the sample differed considerably depending on the calculation method. Initial observations indicate that simply using the initial sample length and platen movement to calculate axial strain (and resulting specimen diameter) does not adequately represent the behaviour of the specimen. Thus, the minimum area approach as first implemented by Roscoe et al. (1964) is recommended. The use of a local versus a global axial digital strain gauge depends on whether the specimen is considered to be a unit cell (as in a conventional compression test) or whether only the region that is actively shearing is of interest.

The following observations were made regarding the strain localization:

- The strain in the sample was uniform until the first slip-stick event occurs. Subsequently, the strain localized, and shear bands formed, bisecting the sample.
- Strain localization was not confined to the region of the sample that necked. Some time after the first shear band formed at the top of the specimen the strain localization progressively moved downwards. This behaviour suggests that the applied stress is distributed to the full specimen and that it is shearing as a unit cell.
- The majority of the shear strain in these, oil-saturated, fused quartz samples occurred during slip events (a sudden drop in deviatoric stress). Before and after the slip-events limited shear strain occurred with no strain localization present.

When considering the results discussed above it should be noted that only two repeat samples of poorly graded fused quartz, saturated with oil were tested at a single confining stress.

5 ACKNOWLEDGEMENTS

The financial assistance of Tensar International Corporation for this study is acknowledged by the authors. Opinions expressed and conclusions presented are solely those of the authors. The authors are grateful to Mr Etienne Gonzales for the translation of the abstract to French.

6 REFERENCES

Bishop, A.W., Henkel, D.J. 1962. *The Measurement of Soil Properties in the Triaxial Test*. Edward Arnold (Publishers) Ltd., London.

Ezzein, F.M., Bathurst, R.J. 2011. A Transparent Sand for Geotechnical Laboratory Modeling. *Geotechnical Testing Journal* 36, 590–601.

Jones, E.M.C., Iadicola, M.A. 2018. *A Good Practice Guide for Digital Image Correlation*. International Digital Image Correlation Society

Marx, D.H. & Zornberg, J.G. 2022. Shear band measurement in transparent sand. *Proceedings of the 20th International Conference on Soil Mechanics and Geotechnical Engineering*, Sydney

Roscoe, K.H., Schofield, A.N., Thurairajah, A. 1964. An Evaluation of Test Data for Selecting a Yield Criterion for Soils. *Laboratory Shear Testing of Soils*. ASTM International, 111–128.

Sadrekarimi, A. 2014. Effect of the Mode of Shear on Static Liquefaction Analysis. *Journal of Geotechnical and Geoenviromental Engineering*. 140,

Stanier, S.A., Blaber, J., Take, W.A., White, D.J. 2016. Improved image-based deformation measurement for geotechnical applications. *Canadian Geotechnical Journal* 53, 727–739.

Vernese, F.J., Lee, K.L. 1977. *Effect of frictionless caps and bases in the cyclic triaxial test (No. S-77-1)*. US Army Engineer Waterways Experiment Station, Vicksburg Mississippi.

Wu, W., Kolymbas, D. 1991. On Some Issues in Triaxial Extension Tests. *Geotechnical Testing Journal* 14, 12.3.2

Yamamuro, J.A., Lade, P.V. 1995. Strain Localization in Extension Tests on Granular Materials. *Journal of Engineering Mechanics* 121.